

Air Force Institute of Technology

AFIT Scholar

Faculty Publications

8-2010

Analytical Solutions for Efficient Interpretation of Single-well Push-pull Tracer Tests

Junqi Huang

John A. Christ

Mark N. Goltz

Air Force Institute of Technology

Follow this and additional works at: <https://scholar.afit.edu/facpub>



Part of the [Environmental Engineering Commons](#), and the [Water Resource Management Commons](#)

Recommended Citation

Huang, J., Christ, J. A., & Goltz, M. N. (2010). Analytical solutions for efficient interpretation of single-well push-pull tracer tests. *Water Resources Research*, 46(8), W08538. <https://doi.org/10.1029/2008WR007647>

This Article is brought to you for free and open access by AFIT Scholar. It has been accepted for inclusion in Faculty Publications by an authorized administrator of AFIT Scholar. For more information, please contact richard.mansfield@afit.edu.

Analytical solutions for efficient interpretation of single-well push-pull tracer tests

Junqi Huang,¹ John A. Christ,² and Mark N. Goltz³

Received 11 December 2008; revised 15 March 2010; accepted 6 April 2010; published 20 August 2010.

[1] Single-well push-pull tracer tests have been used to characterize the extent, fate, and transport of subsurface contamination. Analytical solutions provide one alternative for interpreting test results. In this work, an exact analytical solution to two-dimensional equations describing the governing processes acting on a dissolved compound during a modified push-pull test (advection, longitudinal and transverse dispersion, first-order decay, and rate-limited sorption/partitioning in steady, divergent, and convergent flow fields) is developed. The coupling of this solution with inverse modeling to estimate aquifer parameters provides an efficient methodology for subsurface characterization. Synthetic data for single-well push-pull tests are employed to demonstrate the utility of the solution for determining (1) estimates of aquifer longitudinal and transverse dispersivities, (2) sorption distribution coefficients and rate constants, and (3) non-aqueous phase liquid (NAPL) saturations. Employment of the solution to estimate NAPL saturations based on partitioning and non-partitioning tracers is designed to overcome limitations of previous efforts by including rate-limited mass transfer. This solution provides a new tool for use by practitioners when interpreting single-well push-pull test results.

Citation: Huang, J., J. A. Christ, and M. N. Goltz (2010), Analytical solutions for efficient interpretation of single-well push-pull tracer tests, *Water Resour. Res.*, 46, W08538, doi:10.1029/2008WR007647.

1. Introduction

[2] Single-well push-pull tracer tests, sometimes referred to as single-well injection-withdrawal tests, are designed to capitalize on reactive and chromatographic separation of injected solutes to characterize subsurface properties. They generally employ a single well to inject (“push”) a prepared solution into an aquifer, followed by extraction (“pull”) of the solution from the aquifer using the same well. The injected solution will normally consist of a conservative tracer, along with reacting and/or partitioning compounds. By monitoring concentrations of the extraction solution solutes over time, the physical, chemical and biological properties of the aquifer and those properties governing contaminant transport (e.g., sorption distribution coefficients, degradation rates) may be characterized. The single-well push-pull test provides a reasonable compromise between the localized information obtained via soil coring and the site-averaged information obtained during a partitioning interwell tracer test (PITT) [Istok *et al.*, 2002].

[3] Push-pull tests have been used to measure aquifer physical characteristics like longitudinal dispersivity [Gelhar

and Collins, 1971] and effective porosity [Hall *et al.*, 1991]. They have also been used to quantify solute sorption [Istok *et al.*, 1999; Schroth *et al.*, 2000; Cassiani *et al.*, 2005], the rate of solute degradation [Istok *et al.*, 1997; Haggerty *et al.*, 1998; Snodgrass and Kitanidis, 1998; Istok *et al.*, 2001; Schroth and Istok, 2006], non-aqueous phase liquid (NAPL) saturation [Davis *et al.*, 2002; Istok *et al.*, 2002; Davis *et al.*, 2003, 2005], and rate of mass transfer into zones of immobile water [Haggerty *et al.*, 2001]. In all cases, the desired parameter is obtained through the interpretation of concentration versus time breakthrough data collected during the extraction phase of the push-pull test. Generally, simplified analytical or numerical models are employed to interpret the data by coupling the solution with an optimization algorithm that identifies the parameter set that provides the “best-fit” to the breakthrough data.

[4] Previously reported analytical solutions have generally been restricted to simplified systems and have been limited to the interpretation of longitudinal dispersion [e.g., Gelhar and Collins, 1971], equilibrium sorption [Schroth *et al.*, 2000; Davis *et al.*, 2002], and first-order degradation [e.g., Haggerty *et al.*, 1998; Schroth and Istok, 2006]. Comparisons to experimental results and field-data, however, have demonstrated the importance of dimensionality and rate-limited interphase partitioning (e.g., rate-limited sorption) on model application. Attempts to include additional factors such as transverse dispersion or rate-limited interphase partitioning have, to date, required the implementation of numerical methods [e.g., Haggerty *et al.*, 2001; Schroth *et al.*, 2000; Hellerich *et al.*, 2003]. While capable of modeling these systems, numerical methods add an additional error and level of complexity to the interpretation of

¹Ground Water and Ecosystems Restoration Division, National Risk Management Research Laboratory, U.S. Environmental Protection Agency, Ada, Oklahoma, USA.

²Department of Civil and Environmental Engineering, U.S. Air Force Academy, USAF Academy, Colorado, USA.

³Department of Systems and Engineering Management, Air Force Institute of Technology, Wright-Patterson Air Force Base, Ohio, USA.

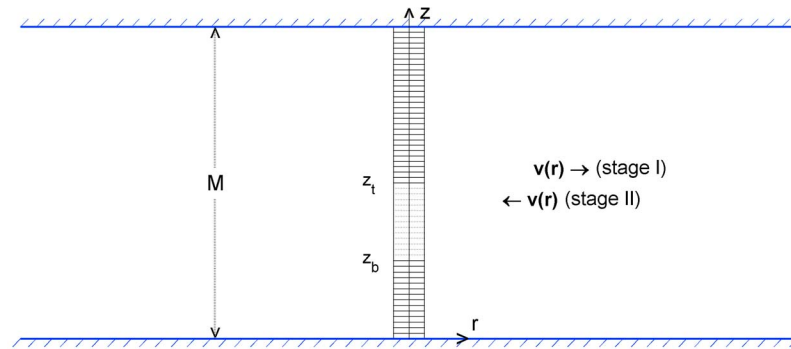


Figure 1. Conceptual model and coordinate system.

the results due to numerical errors and difficulties associated with implementing numerical methods for the interpretation of these tests, which were originally derived as simplified aquifer characterization techniques [Schroth *et al.*, 2000].

[5] In this study, a new analytical solution, designed to overcome the limitations of existing single-well push-pull model solutions, is developed. The model accounts for advection, longitudinal and transverse (vertical) dispersion, first-order degradation, and rate-limited interphase partitioning during nonuniform, steady radial flow in a homogeneous, confined aquifer. The solution can accommodate a modified push-pull test, where tracer is not injected over the entire confined aquifer depth, thereby allowing for estimation of the transverse dispersivity in the vertical direction. Although relatively novel, there have been field implementations of injection wells configured (using packers) to release tracer over a portion of a fully penetrating well screen [e.g., Brooks *et al.*, 2002]. Employment of the solution to estimate NAPL saturations based on partitioning and non-partitioning tracers is designed to overcome limitations of previous efforts by including rate-limited mass transfer. This solution provides a novel addition to the currently available methods for interpreting single-well push-pull test results.

2. Model Development

[6] A number of analytical solutions have been derived to describe radially convergent or divergent flow and transport resulting from operation of a single extraction or injection well [Hoopes and Harleman, 1967; Gelhar and Collins, 1971; Pickens and Grisak, 1981; Tang and Babu, 1979; Tang and Peaceman, 1987; Moench, 1989; Zlotnik and Logan, 1996; Schroth *et al.*, 2000; Cassiani *et al.*, 2005]. These solutions have generally employed simplifying assumptions such as one-dimensional flow, linear equilibrium sorption, constant tracer injection, and zero or first-order degradation. Chen [1985], however, derived a solution for a fully penetrating injection well with advection and simultaneous Fickian diffusion into adjacent low permeability strata. Chen [1987] derived a second solution to include Cauchy boundary conditions at the injection well screen, facilitating the simulation of more realistic mass loading conditions at the injection well. Huang and Liu [1986] also derived a solution for radial transport in dual porosity media, which facilitated the

simulation of mass exchange in fractured systems. In all cases, however, the tracer injection was assumed to be over the entire aquifer depth, preventing the characterization of transverse dispersivity in the vertical direction. Also, previous solutions that incorporated rate-limited sorption or partitioning into immobile zones were for injection or extraction only, not for both, as would be necessary to model a push-pull test [e.g., Goltz and Oxley, 1991]. The following derivation overcomes these limitations and accounts for advection, longitudinal and transverse (vertical) dispersion, first-order degradation and rate-limited interphase partitioning. Constant concentration and third-type (flux) boundary conditions are employed at the well screen. Flow is assumed to be in the radial direction only with mechanical dispersion occurring in the longitudinal (radial) and transverse (vertical) directions. Analytical solutions are obtained using Laplace and Finite Fourier transforms. The solution is derived assuming a two-stage test. During stage 1, the flow is divergent as water is injected into the confined aquifer and tracer is released over a portion of the fully penetrating well screen. In stage 2, the flow is convergent as the well extracts water from the aquifer and tracer solutions are recovered through the screened section of the well. Figure 1 depicts the modeled scenario where in a fully screened well of length M , tracer is released from z_b to z_t .

2.1. Governing Equations

[7] The following equations describe advective/dispersive transport of a reacting and sorbing compound in a radially symmetric, horizontal flow field:

$$r \left(\theta \frac{\partial C}{\partial t} + \rho_b \frac{\partial S}{\partial t} \right) = a_L q \frac{\partial^2 C}{\partial r^2} + q \frac{\partial C}{\partial r} + a_T q \frac{\partial^2 C}{\partial z^2} - r \theta \lambda C - r \rho_b \lambda S \quad (1)$$

$$\frac{\partial S}{\partial t} = -\alpha(S - k_d C) - \lambda S \quad (2)$$

Equation (1) is the two-dimensional (r - z) advection-dispersion equation in radial coordinates, assuming radial symmetry for a sorbing and reacting compound [Bear, 1979], and equation (2) describes sorption of the compound onto aquifer solids, where rate-limited sorption is described as a first-order process. C is the compound concentration in the liquid phase, S is the concentration in the solid phase,

θ is the aquifer porosity, ρ_b is the aquifer bulk density, $q = Q/2\pi M$ where Q is the well flow-rate, M is the confined aquifer thickness, a_L and a_T are the longitudinal and transverse dispersivity, respectively, λ is a first-order decay constant, α is the non-equilibrium sorption first-order mass transfer rate coefficient, and k_d is the adsorption partitioning coefficient. Equations (1) and (2) are solved according to the following initial and boundary conditions during stage 1 ("push") and stage 2 ("pull") of the single-well push-pull test:

Stage 1 (injection):

$$C = S = 0, \quad t = 0 \quad (3a)$$

$$-\sigma a_L \frac{\partial C}{\partial r} + C = \begin{cases} C_0, & r = r_w, z_b \leq z \leq z_t \\ 0, & r = r_w, 0 \leq z < z_b, z_t < z \leq M \end{cases} \quad (3b)$$

$$C = 0, \quad r \rightarrow \infty, \quad 0 \leq z \leq M \quad (3c)$$

$$\frac{\partial C}{\partial z} = 0, \quad r_w \leq r < \infty, \quad z = 0, \quad M \quad (3d)$$

Stage 2 (extraction)

$$C = C_l(r, z, t_1), \quad S = S_l(r, z, t_1), \quad t = 0 \quad (4a)$$

$$\frac{\partial C}{\partial r} = 0, \quad r = r_w, \quad 0 \leq z \leq M \quad (4b)$$

$$C = 0, \quad r \rightarrow \infty, \quad 0 \leq z \leq M \quad (4c)$$

$$\frac{\partial C}{\partial z} = 0, \quad r_w \leq r < \infty, \quad z = 0, \quad M \quad (4d)$$

where C_0 is the concentration of injected tracer, r_w is the well radius, z_b and z_t are the bottom and top elevation of the tracer injection segment of the well, respectively, σ is a control flag with values 1 or 0 for constant flux or constant concentration boundary conditions respectively, and $C_l(r, z, t_1)$ and $S_l(r, z, t_1)$ are the initial distributions of liquid and solid phase compound concentrations, respectively, following the completion of stage 1 at time t_1 . Note from equation (3b) that although the aquifer thickness is M and the well is screened over the entire aquifer thickness, tracer injection is only over the vertical interval between z_t and z_b (where $z_t - z_b \leq M$).

2.2. Transformed and Real-Time Solutions

[8] Solution of equations (1) and (2) combine Laplace transforms with respect to t (\bar{C}) and Finite Fourier Cosine transforms with respect to z (\hat{C}) with substitutions as shown in Appendix A to simplify the problem to the well known Airy equation. Parameterization of the general solution using the transformed boundary conditions for stage 1 (equation (3), see Appendix A) leads to a transformed concentration in the aqueous phase:

$$\hat{C}_1(r, n, p) = \frac{C_0}{p} \Lambda(n) e^{\frac{r-r_w}{2a_L}} \frac{Ai(x)}{\gamma_1 Ai(x_w) - \gamma_2 Ai'(x_w)} \quad (5)$$

and solid phase:

$$\hat{S}_1(r, n, p) = \frac{\alpha k_d}{p + \lambda + \alpha} \hat{C}_1(r, n, p) \quad (6)$$

where all parameters in this section may be found in the appendices. The subscript 1 signifies the solutions are for stage 1 of the single-well push-pull test, and $\gamma_1 = 1 - \sigma/2$, $\gamma_2 = \sigma a_L^{2/3} f^{1/3}$ and $x_w = a_L^{-1/3} \left(\frac{1}{4a_L} + r_w f + N \right) f^{-2/3}$.

[9] Following a similar methodology for stage 2, where the nonzero initial condition established at the end of stage 1 (equation (4a)) is considered using Green's function, and the transformed boundary conditions (equations (4)) are used to parameterize the general solution, the transformed stage 2 concentration in the aqueous phase may be written (see Appendix A):

$$\hat{C}_2(r, n, p) = c_1(n, p) e^{-\frac{r}{2a_L}} Ai(x) + H(r, n, p) \quad (7)$$

where

$$c_1 = -\frac{\pi}{\gamma} \frac{Bi(x_w) - 2\gamma Bi'(x_w)}{Ai(x_w) - 2\gamma Ai'(x_w)} \int_{r_w}^{\infty} e^{\frac{r}{2a_L}} Ai(x) g(r, n, p) dr$$

$$H = \frac{\pi}{\gamma} e^{-\frac{r}{2a_L}} \left[Ai(x) \int_{r_w}^r e^{\frac{r}{2a_L}} Bi(x) g(r, n, p) dr + Bi(x) \int_r^{\infty} e^{\frac{r}{2a_L}} Ai(x) g(r, n, p) dr \right]$$

and $\gamma = a_L^{2/3} f^{1/3}$. Equation (7) provides a transformed solution for the aqueous phase concentration during stage 2 (pull) of the push-pull test.

[10] Given that single-well push-pull tests employ solute concentrations extracted during stage 2 of the test to obtain aquifer parameters, it is necessary to quantify the concentration at the extraction well ($r = r_w$). For this condition, equation (7) simplifies:

$$\hat{C}_2(r_w, n, p) = \frac{2e^{-\frac{r_w}{2a_L}}}{Ai(x_w) - 2\gamma Ai'(x_w)} \int_{r_w}^{\infty} e^{\frac{r}{2a_L}} Ai(x) g(r, n, p) dr \quad (8)$$

or

$$\hat{C}_2(r_w, n, p) = \frac{e^{-\frac{r_w}{2a_L}}}{q} \int_{r_w}^{\infty} e^{\frac{r}{2a_L}} \bar{F}_2(r, n, p) r \cdot \left[\theta \hat{C}_1(r, n, t_1) + \frac{\rho_b \alpha}{p + \lambda + \alpha} \hat{S}_1(r, n, t_1) \right] dr \quad (9)$$

with $\bar{F}_2(r, n, p) = \frac{2Ai(x)}{Ai(x_w) - 2\gamma Ai'(x_w)}$ or using from Appendix B, $\bar{F}_2(r, n, p) = p \bar{F}_{CF}(r, n, p)$.

[11] Comparison with actual field results, however, requires inversion of these transformed solutions to real time and space. To obtain the aqueous concentration solution in real time, equations (5)–(9) may be inverted following the methods outlined in Appendices B and C. For a constant concentration boundary condition ($\sigma = 0$), equation (5) may be written in real time:

$$\hat{C}_1(r, n, t) = C_0 \Lambda(n) e^{\frac{r-r_w}{2a_L}} F_{CC}(r, n, t) \quad (10)$$

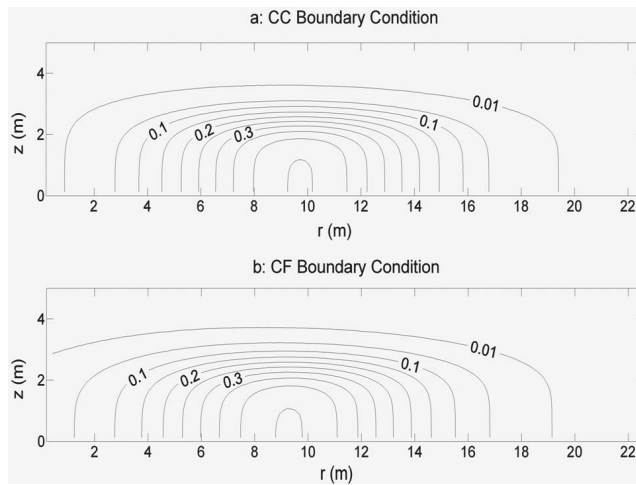


Figure 2. Concentration contour (mg/L) in the z - r plane on day 5 of injection for (a) constant concentration (CC) boundary condition and (b) constant flux (CF) boundary condition at the injection well, for parameter values in Table 1.

For a constant flux boundary condition ($\sigma = 1$) equation (5) becomes

$$\hat{C}_1(r, n, t) = C_0 \Lambda(n) e^{\frac{r-r_w}{2aL}} F_{CF}(r, n, t) \quad (11)$$

where $F_{CC}(r, n, t)$ (equation (B9)) and $F_{CF}(r, n, t)$ (equation (C6)) are defined in Appendices B and C. A special case is also given in Appendix A for the scenario where a tracer is injected for a pulse length t_s , less than t_1 , the length of water injection during stage 1.

[12] The solid phase stage 1 concentration in real time can be obtained by inverting equation (6):

$$\begin{aligned} \hat{S}_1(r, n, t) &= \alpha k_d \int_0^t e^{-(t-\tau)(\lambda+\alpha)} \hat{C}_1(r, n, \tau) d\tau \\ &= C_0 \alpha k_d \Lambda(n) e^{\frac{r-r_w}{2aL}} F_{conv}(r, n, t) \end{aligned} \quad (12)$$

where $F_{conv}(r, n, t)$ is given in Appendix A.

[13] To obtain the analytical solutions for concentrations in the aqueous and solid phase in real time and space during stage 1 of the single-well push-pull test the inverse Finite Fourier Cosine transform is applied:

$$C_1(r, z, t) = \frac{1}{M} \hat{C}_1(r, 0, t) + \frac{2}{M} \sum_{n=1}^{\infty} \hat{C}_1(r, n, t) \cos\left(\frac{n\pi z}{M}\right) \quad (13a)$$

$$S_1(r, z, t) = \frac{1}{M} \hat{S}_1(r, 0, t) + \frac{2}{M} \sum_{n=1}^{\infty} \hat{S}_1(r, n, t) \cos\left(\frac{n\pi z}{M}\right) \quad (13b)$$

where \hat{C}_1 and \hat{S}_1 are as given previously.

[14] Although the same methodology could be applied to invert equation (7), equation (9) is considered here due to the primary interest in aqueous phase concentrations at the extraction well during the push-pull test. Employing the Laplace transform of the derivative and the convolution

principle as shown in Appendix A, the transformed solution at the extraction well in real time may be written

$$\begin{aligned} \hat{C}_2(r_w, n, t) &= e^{-\frac{r_w}{2aL}} \int_{r_w}^{\infty} e^{\frac{r}{2aL}} r [\theta F_2(r, n, t) \hat{C}_1(r, n, t_1) \\ &\quad + \Phi(r, n, t) \hat{S}_1(r, n, t_1)] dr \end{aligned} \quad (14)$$

where $\Phi(r, n, t)$ (equation (A11)) is given in Appendix A.

[15] Using the inverse Finite Fourier Cosine transform, the final analytical solution for the solute concentration at the extraction well during stage 2 of the single-well push-pull test is

$$C_2(r_w, z, t) = \frac{1}{M} \hat{C}_2(r_w, 0, t) + \frac{2}{M} \sum_{n=1}^{\infty} \hat{C}_2(r_w, n, t) \cos\left(\frac{n\pi z}{M}\right) \quad (15)$$

where \hat{C}_2 is as given in equation (14). Note that the concentration given by equation (15) is a function of the aqueous and solid phase concentration distribution at the completion of stage 1 (when $t = t_1$). Equation (15) provides an analytical solution that may be combined with optimization algorithms to obtain aquifer parameters (i.e., dispersivities, k_d , α , λ) from data obtained for single-well push-pull tracer tests in confined aquifers with the injection compound released over only a portion of the well screen and rate-limited mass transfer between the aqueous and immobile (solid and non-aqueous phase liquid) phases. Equation (15) has been implemented in a computer program as described below, which has been made available by the authors (see auxiliary material) to facilitate its use when interpreting push-pull experimental results.¹

2.3. Numerical Evaluation of Solution

[16] The International Mathematical and Statistical Library (IMSL) subroutines DQDAG and DQDAGI [International Mathematical and Statistical Library, 2006] based on Gauss-Kronrod rules [Piessens et al., 1983] are used to numerically evaluate the integrals which appear in the solutions (equations (13) and (15)). The Airy functions, $Ai(z)$ and $Bi(z)$, and their derivatives, $Ai'(z)$ and $Bi'(z)$, are also available in IMSL. For example, equation (13a) was evaluated using the IMSL routines to determine the dissolved concentrations of a sorbing, degrading tracer for the baseline parameter values listed in Table 1. Figures 2a and 2b show aqueous phase tracer concentration contours in the r - z plane after 5 days of water injection (that is, $t_1 = 5d$), assuming constant concentration and constant flux boundary conditions, respectively, at the well. The tracer is released for $t_s = 3$ days through a segment of the well screen located at $r = r_w$ between $z_b = 0$ m and $z_t = 2.5$ m. Clearly, the solution provides for an efficient method to elucidate solute concentrations surrounding a partially screened push-pull well at a given point in time. It is also worth noting that this concentration profile serves as the initial condition for the “pull” stage of the test.

3. Model Verification and Validation

[17] The analytical solutions developed here were verified by comparing them with solutions obtained using an explicit

¹Auxiliary materials are available in the HTML. doi:10.1029/2008WR007647.

Table 1. Base Line Parameter Values Used for Simulations

Parameter	Value
a_L (m)	2.0
a_T (m)	0.02
θ	0.3
ρ_b (kg/L)	1.67
α (d ⁻¹)	0.02
k_d (L/kg)	3.0
λ (d ⁻¹)	0.001
r_w (m)	0.2
M (m)	5.0
z_t (m)	2.5
z_b (m)	0.0
C_0 (mg/L)	1.0
Q_1^a (m ³ /d)	120.0
Q_2^a (m ³ /d)	120.0
t_1^b (d)	5.0
t_s^b (d)	3.0

^a Q_1 and Q_2 are the wells' pumping rates in stages 1 and 2, respectively.

^bHere t_1 is the total water injection time during stage 1, and t_s is the time tracer is released during stage 1.

finite difference numerical code to approximate equations (1) and (2), subject to the appropriate initial and boundary conditions. The finite difference scheme used a grid spacing in the r - and z -directions of 0.2 m (Δr) and 0.25 m (Δz), respectively. Based on numerical stability criteria [Zheng and Wang, 1999], the time step (Δt) was set to

$$\Delta t = 2 \times 10^{-5} < \min \left(\frac{r_w \Delta r \theta}{q}, \frac{r_w \Delta r^2 \theta}{2a_L q}, \frac{r_w \Delta z^2 \theta}{2a_T q}, \frac{1}{\lambda} \right) \quad (16)$$

[18] Figure 3 compares the analytical and numerical solutions for the values provided in Table 1 for constant con-

centration (CC) and constant flux (CF) boundary conditions. Figure 3 shows concentration as a function of time for $z = z_t + (M - z_t)/2 = 3.75$ m at the extraction well ($r = r_w$). Note the low concentrations at the well ($\sim 10^{-3}$ mg/L), due to the fact that concentrations are measured at a location above the top of the well screen, and the value of transverse dispersivity in the vertical direction is low ($a_T = 0.02$ m). The excellent match with the numerical solution gives confidence in the correctness of the analytical solution.

[19] To further extend this validation, the model may be compared to data from an actual field site. However, given the lack of readily available field data for this study, a commonly employed numerical model (MODFLOW/MT3DMS) was used to replicate push-pull concentration data from a synthetic field site with heterogeneous hydraulic conductivity (mean hydraulic conductivity = 20 m/d). The method of Taskinen *et al.* [2008] was used to generate heterogeneous hydraulic conductivity fields with specified correlation lengths for use in the numerical modeling. Transforming the MODFLOW [McDonald and Harbaugh, 1988] and MT3DMS [Zheng and Wang, 1999] domains from a three-dimensional Cartesian system to a two dimensional cylindrical system using scaling factors, r and 2π , to achieve computational efficiencies, tracer concentrations at the extraction well ($r = r_w, z = z_t + (M - z_t)/2$) were calculated and compared with the concentrations obtained using the analytical solution, which assumes homogeneity, for a constant flux (CF) boundary condition. The CF boundary condition was used for the analytical model as it has the advantage of preserving mass balance. The analytical solution was compared with numerical simulations that were based on specified mass loading at the injection well.

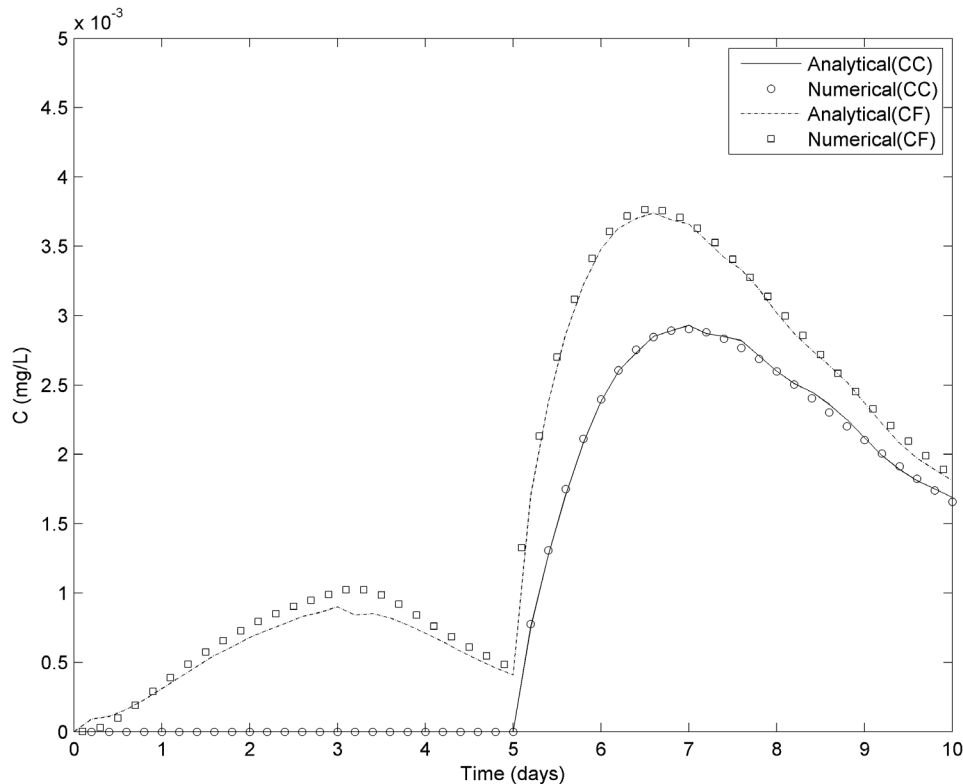


Figure 3. Comparison of results using analytical and numerical solutions for CC and CF boundary conditions.

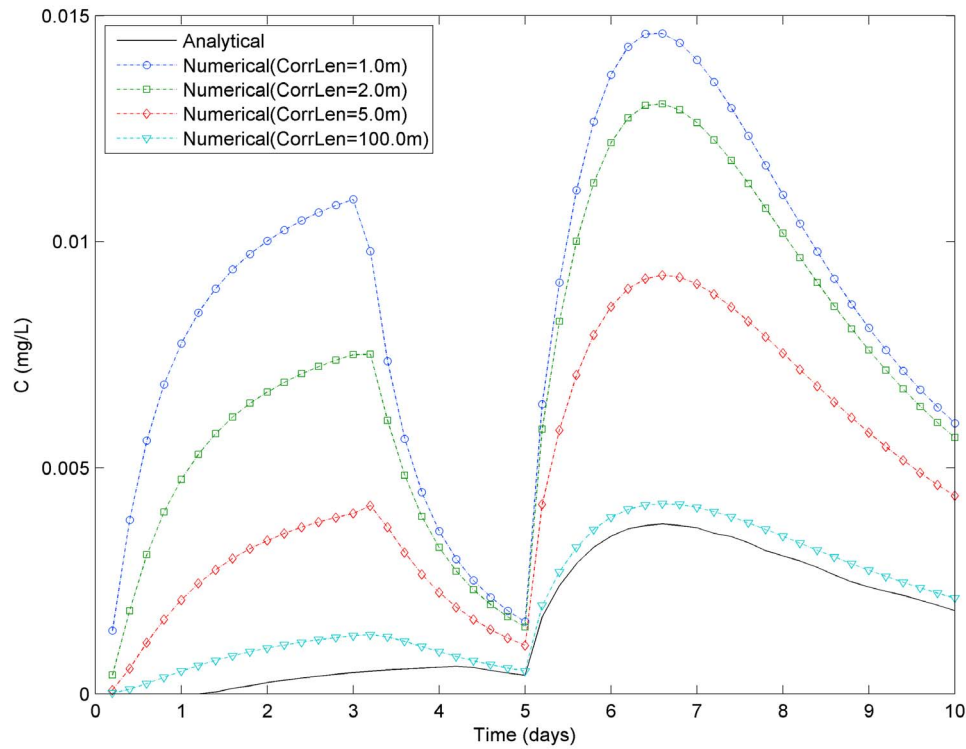


Figure 4. Comparison of tracer concentrations at the extraction well ($r = r_w$, $z = z_t + (M - z_t)/2$) assuming homogeneity (analytical solutions) and heterogeneity (correlation length of hydraulic conductivity = 1.0, 2.0, 5.0 and 100.0 m) for constant flux (CF) boundary conditions at the injection well, for parameter values in Table 1.

Figure 4 demonstrates the analytical solution assuming a homogeneous system only provides a reasonable approximation to the heterogeneous synthetic field site data when the correlation length for the heterogeneous system is relatively large. Thus, application of this methodology in heterogeneous permeability fields with poor correlation structure should be performed with caution.

4. Sensitivity Analysis

[20] Inverse modeling is typically used to estimate system parameters from observations. To guide inverse modeling, it is helpful to define metrics to quantify the importance of the fitted parameters. One such metric is a composite scaled sensitivity (CSS) [Hill, 1992; Anderman *et al.*, 1996; Hill *et al.*, 1998] that quantifies the dependency of a parameter to be estimated (P) on observations. For the push-pull system, CSS may be defined as [Hill, 1992; Anderman *et al.*, 1996; D'Agnese *et al.*, 1996; Hill *et al.*, 1998]

$$CSS(P) = \left[\frac{1}{N} \sum_{i=1}^N \left(w_i (P \partial C^o(t_i) / \partial P)^2 \right) \right]^{1/2} \quad (17)$$

where $C^o(t_i)$ is the observed concentration at time t_i ; N is the total number of observations (i.e., concentration measurements), and w_i is the weight of the i th observation, where the weight is the inverse of a subjective estimate of the variance of the measurement error (here $w_i = 1/C^o(t_i)^2$). Increasing CSS values indicate increasing information about the value

of parameter P that can be gleaned from the concentration measurements.

[21] In the push-pull experimental procedure, $C^o(t_i)$ is defined as the average concentration at time t_i along some segment of the extraction well screen rather than the entire screen length. Estimating concentration along a section of the screen length using e.g., a multilevel sampling well located adjacent to the fully screened extraction well, provides for the ability to estimate transverse dispersivity, as will be discussed in the following section. For example, averaging over the well screen segment directly above the tracer injection zone (i.e., $z = z_t$ to M):

$$C^o(t_i) = \frac{1}{M - z_t} \int_{z_t}^M C_2(r_w, z, t_i) dz \quad (18)$$

[22] Table 2 lists the CSS for parameters estimated in the push-pull model in the subsequent section. As will be described in the next section, the model is used to estimate dispersivities (a_L and a_T), adsorption parameters (k_d and α), and parameters describing distribution of a NAPL (θ , average NAPL saturation (S_n), and NAPL-water partitioning tracer first-order mass transfer rate coefficient (α_{NAPL})). As indicated for the conditions listed in Table 1, the porosity θ has the highest CSS and the decay constant λ the lowest. Depending on the optimization method, a relatively low CSS would result in low confidence in the parameter estimate. Note, however, that the CSS values in Table 2 were determined for the specific set of operating conditions in Table 1, and under other conditions the relative magnitude of the

Table 2. Composite Scaled Sensitivity to Selected Parameters for Table 1 Conditions

	Group								
	Adsorption			Dispersion			NAPL		
	α	k_d	λ	θ	a_L	a_T	θ	S_n	α_{NAPL}
CSS	0.026	2.396	0.000007	0.326	2.20	0.011	0.762	0.011	0.005
Rank	2	1	3	2	1	3	1	2	3

CSS values would likely be different. For example, the parameter values listed in Table 1 suggest the time constant for decay is on the order of 1000 days, which is much larger than the duration of the push-pull test, leading to a relatively low decay constant CSS.

[23] To better understand parameter sensitivity, the CSS to two parameters, a_L and a_T , was examined. Well pumping rates and the vertical location at which concentrations were measured (z) were varied. Figures 5a and 5b show the CSS to a_L and a_T , respectively, for varying well pumping rates. Figure 5b shows that at lower pumping rates, the CSS to a_T increases, meaning that at lower well pumping rates, it is relatively easier to elicit information about the value of a_T from concentration measurements. However, Figure 5a shows that as the pumping rate decreases, the CSS to a_L decreases, implying the simultaneous estimate of a_L and a_T will require selection of a pumping rate that is low enough to provide a good estimate of a_T yet high enough to provide a good estimate of a_L . Figures 5c and 5d show how the vertical sampling location affects the CSS to a_L and a_T , respectively. The CSS to both a_L and a_T increases as the

sampling location gets further from the top of the well screen (recall $z_t = 2.5$ m). Finally, note from Figure 5 that the CSS to a_L is orders of magnitude greater than the CSS to a_T , indicating that the estimate of a_L will, at least for the parameter values in Table 1, be significantly better than the estimate of a_T . Another parameter that may be used to determine whether parameters can be estimated uniquely is the correlation coefficient. Defining the elements of the sensitivity matrix as

$$S_{ij} = \frac{\partial C^0(t_i)}{\partial P_j} \tag{19}$$

where $C^0(t_i)$ is the concentration at time t_i and P_j is the j th parameter, the correlation coefficients may be calculated using the covariance matrix $\text{cov}(S_{i,j})$ [Rodgers and Nicewander, 1988]:

$$R = \frac{\text{cov}(S_{i,j})}{\sqrt{\text{cov}(S_{i,i})\text{cov}(S_{j,j})}} \tag{20}$$

[24] The correlations between parameters are shown in Table 3. Hill *et al.* [1998] noted that correlations exceeding 0.95 indicate that it may be difficult to independently estimate parameter values. Note from Table 3 that, at least for the example parameter values in Table 1, all correlation coefficients for the dispersivities and sorption parameters are less than 0.95, while the correlation coefficients for the NAPL distribution parameters are all significant (with the

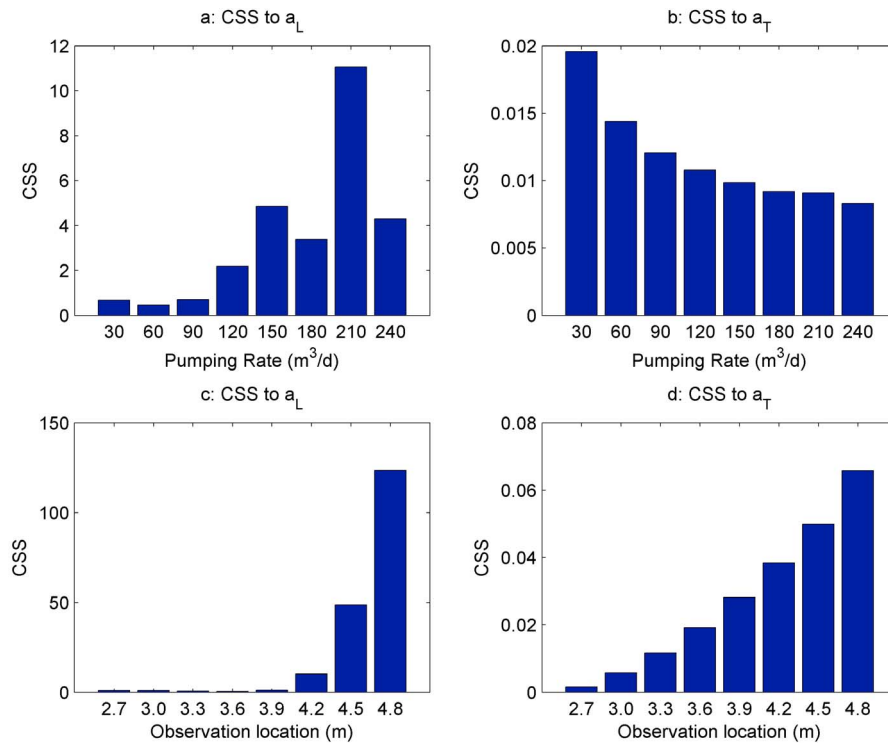


Figure 5. Sensitivity analysis CSS to (a) a_L and (b) a_T as a function of pumping rate and CSS to (c) a_L and (d) a_T as a function of z . Note that the well screen extends from $z = 0$ to 2.5 m.

Table 3. Correlation Coefficients Between Parameters for Table 1 Conditions

Adsorption			Dispersion				NAPL				
Parameter	α	k_d	λ	Parameter	θ	a_L	a_T	Parameter	θ	S_n	α_{NAPL}
α	1.00	-0.62	0.24	θ	1.00	-0.13	0.21	θ	1.00	-0.98	-0.93
k_d	-0.62	1.00	0.43	a_L	-0.13	1.00	-0.82	S_n	-0.98	1.00	0.99
λ	0.24	0.43	1.00	a_T	0.21	-0.82	1.00	α_{NAPL}	-0.93	0.99	1.00

correlation coefficients for $\theta - S_n$ and $\alpha_{NAPL} - S_n$ both greater than 0.95).

5. Applications

[25] In this section we develop procedures and simplified model equations that can be used to estimate parameter values from field test tracer signals. Applications discussed below include estimation of dispersivities, sorption parameters, and non-aqueous phase liquid (NAPL) saturation examples. As noted earlier, due to its relatively low CSS caused by the extended half-life relative to the tracer test, estimation of the degradation rate constant is problematic for the Table 1 parameter values used here. Therefore, estimation of the degradation rate constant (λ) will not be attempted for the Table 1 conditions being evaluated in this study. Simplified methods of determining first-order degradation rate constants with push-pull tests have been presented previously, however [e.g., Haggerty et al., 1998; Schroth and Istok, 2006]. Each application example in this section employs a genetic algorithm coupled to the analytical solution to quantify model parameters for synthetic single-well push-pull tracer data. Simplified solutions for each application are derived first to aid in the implementation of the model in specific site characterization scenarios.

5.1. Dispersivity Measurement

[26] To measure a_L and a_T a non-sorbing, non-degrading, conservative tracer (i.e., $\lambda = \alpha = k_d = 0$) should be used. For these conditions, where transport is governed by advection and dispersion only, the transport equation solutions for both stages may be simplified as follows. During stage 1 the intermediate function F_{CC} in equation (10) can be expressed as

$$F_{CC}(r, n, t) = e^{-\frac{1}{2a_L}(r-r_w)\sqrt{1+4a_L N}} - \frac{2}{\pi} \int_0^\infty \frac{e^{-\xi^2 t}}{\xi} \Psi(r, n, \xi) d\xi \quad (21)$$

and F_{CF} in equation (11) as

$$F_{CF}(r, n, t) = 2e^{-\frac{1}{2a_L}(r-r_w)\sqrt{1+4a_L N}} - \frac{4}{\pi} \int_0^\infty \frac{e^{-\xi^2 t}}{\xi} \Omega(r, n, \xi) d\xi \quad (22)$$

where Ψ and Ω have the same form as in Appendices A and B, except $h = \theta\xi^2/q$. During stage 2, the stage 1 solution at $t = t_1$ provides the initial condition. Using the simplified equations (21) and (22), the concentration at the extraction well ($r = r_w$) previously expressed in equation (14) can now be written

$$\hat{C}_2(r_w, n, t) = \frac{\theta e^{-\frac{r_w}{2a_L}}}{q} \int_{r_w}^\infty e^{\frac{r}{2a_L}} r F_2(r, n, t) \hat{C}_1(r, n, t_1) dr \quad (23)$$

where $\hat{C}_1(r, n, t_1)$ is as given in equation (A6) or (A7) (with $t = t_1$), $F_2(r, n, t)$ has the form

$$F_2(r, n, t) = \frac{4}{\pi} \int_0^\infty \xi e^{-\xi^2 t} \Omega(r, n, \xi) d\xi \quad (24)$$

and $h = \theta\xi^2/q$. Inverting the Finite Fourier Cosine transform:

$$C_2(r_w, z, t) = \frac{1}{M} \hat{C}_2(r_w, 0, t) + \frac{2}{M} \sum_{n=1}^\infty \hat{C}_2(r_w, n, t) \cos\left(\frac{n\pi z}{M}\right) \quad (25)$$

and the average concentration integrated over the entire well screen depth is

$$C_2^{ave}(r_w, t) = \frac{1}{M} \int_0^M C_2(r_w, z, t) dz \quad (26)$$

[27] Note that measuring concentrations averaged over the well screen depth won't provide any information useful in determining the transverse dispersivity because the second term on the right hand side of (25), which contains information on a_T , vanishes upon averaging. Thus, it is necessary to sample over a fraction of the aquifer depth in order to obtain information necessary to estimate a_T .

[28] The importance of having a model that incorporates transverse dispersion in the vertical direction is demonstrated in Figure 6. In Figure 6, for the Table 1 parameter values, tracer concentrations at a sampling location above the extraction well screen ($r = r_w$, $z = z_t + (M - z_t)/2 = 3.75$ m) are simulated for various values of transverse dispersivity. Since the sampling location is above the top of the well screen, if there were no transverse dispersion ($a_T = 0.0$ m), concentrations would be zero at all times. As can be seen from Figure 6, transverse dispersion results in concentrations that are significantly greater than zero, and the greater the transverse dispersivity, the higher the concentrations that are simulated at a sampling location above the top of the injection-extraction well screen.

5.2. Sorption Parameters Measurement

[29] Prior to evaluating the sorption parameter values, it is assumed that the longitudinal and transverse dispersivity values have been estimated as described in the preceding section. With transverse dispersivity quantified, tracer injection during Stage 1 may be over the entire aquifer depth, so $\Lambda(n) = 0$ in equation (11) for all $n > 0$ and $\Lambda(0) = M$, which simplifies equations (10) and (11) for constant concentration:

$$C_1(r, t) = C_0 \exp\left(\frac{r - r_w}{2a_L}\right) (F_{CC}(r, 0, t) - F_{CC}(r, 0, t - t_s)) \quad (27)$$

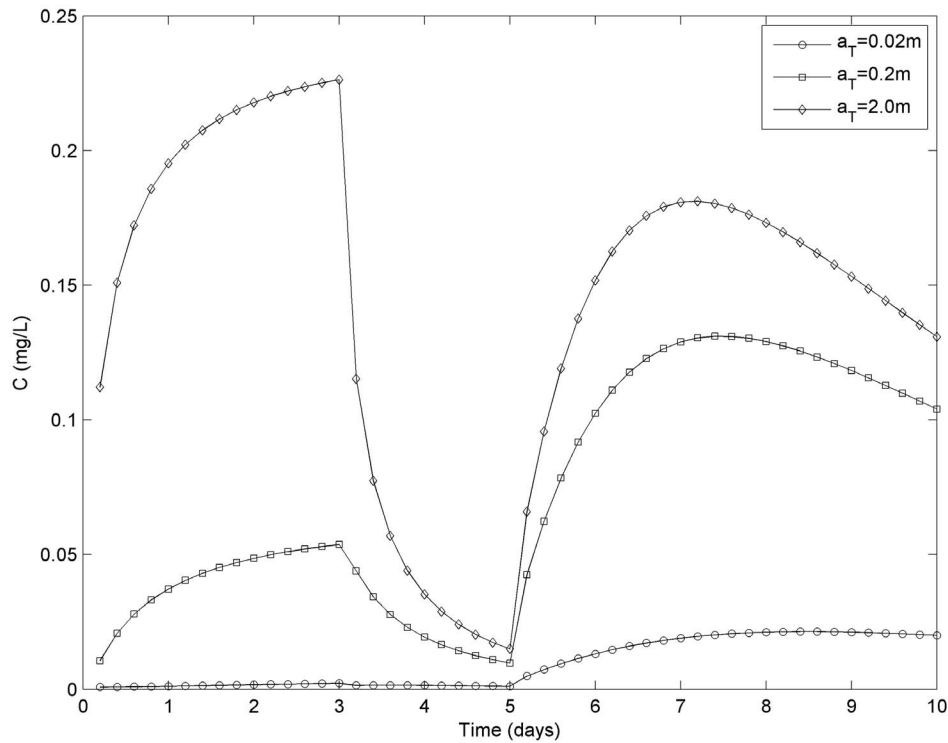


Figure 6. Comparison of simulated breakthrough concentrations at the extraction well ($r = r_w, z = 3.75$ m) for different vertical transverse dispersivities and CF boundary conditions.

and for constant flux boundary conditions:

$$C_1(r, t) = C_0 \exp\left(\frac{r - r_w}{2a_L}\right) (F_{CF}(r, 0, t) - F_{CF}(r, 0, t - t_s)) \quad (28)$$

These equations may be solved for radial transport when injecting a sorbing solute through a fully screened well to obtain two sorption parameter estimates: α (the first-order sorption rate constant) and k_d (sorption partition coefficient). Equation (15) is still applicable to describe the concentration in the extraction well during Stage 2 (C_2), except the initial concentration of stage II is now given by equations (27) and (28), respectively, for constant concentration and constant flux boundary conditions. The sorbed concentration for this application is expressed

$$S_1(r, t) = \alpha k_d \int_0^t e^{-(t-\tau)(\lambda+\alpha)} C_1(r, \tau) d\tau \quad (29)$$

5.3. NAPL Saturation Measurement

[30] Given the novelty of this application it is important to outline in more detail the previous efforts to quantify in situ NAPL saturations using single-well partitioning tracer study results. Partitioning tracers were initially proposed for use in interwell tracer tests [Jin *et al.*, 1995] as an effective method for quantifying the average non-aqueous phase liquid (NAPL) saturation within a NAPL source zone. More recently, work has focused on adaptation of this methodology to the single-well push-pull tracer technology [e.g., Istok *et al.*, 2002]. This methodology evolved from the petroleum engineering literature where it was proposed for

the identification of residual oil [e.g., Tomich *et al.*, 1973]. Recent environmental applications have focused on the interpretation of single-well push-pull partitioning and non-partitioning tracer signals to identify NAPL contaminant [Istok *et al.*, 2002; Davis *et al.*, 2002, 2005]. Istok *et al.* [2002] employed a single-well push-pull test to quantify TCE saturations in bench-scale model aquifers and at a field site in Cincinnati, OH. A similar test was employed by Davis *et al.* [2002, 2005], which relied on injection of a conservative tracer and radon-free tap water. During extraction, the conservative tracer and a naturally occurring partitioning tracer, Radon-222, were monitored. The model of Schroth *et al.* [2000] was then used to interpret the extraction signals of the partitioning and non-partitioning tracers to compute a retardation coefficient ($R = 1 + \rho_b/\theta K$), which could then be combined with the known equilibrium partitioning tracer-NAPL partitioning coefficient (K) to compute the average NAPL saturation (S_n):

$$S_n = \frac{R - 1}{R + K - 1} \quad (30)$$

[31] Application of (30) requires the assumption that the mass transfer of the partitioning tracer to the NAPL is rapid enough that rate-limitations may be ignored. Previously reported results [Istok *et al.*, 2002; Davis *et al.*, 2002, 2005], however, suggest this is a poor assumption in single-well push-pull tests and that the dispersion observed in the partitioning tracer extraction signal is likely caused by both non-equilibrium effects and heterogeneous distribution of NAPL. Modeling these effects has generally required the

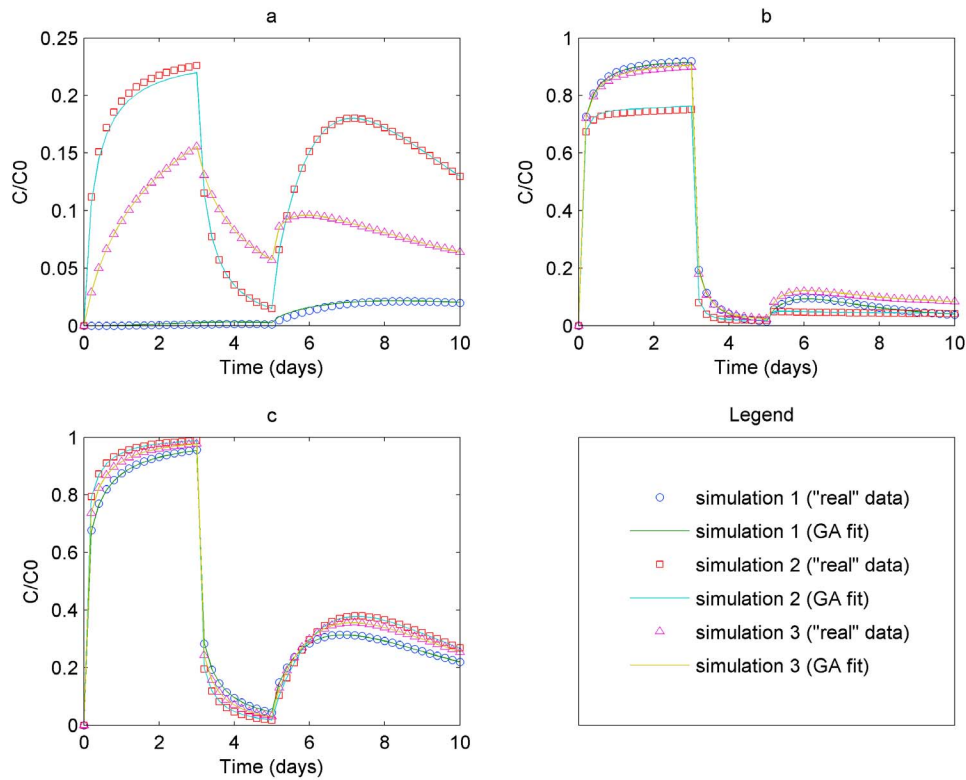


Figure 7. Comparison of “real” concentration data from example with simulated data using GA-obtained parameter values for (a) longitudinal and transverse dispersivities (a_L , a_T), (b) sorption parameters (α , k_d), and (c) NAPL distribution parameters (θ , S_n , α_{NAPL}).

implementation of numerical models [e.g., *Schroth et al.*, 2000].

[32] The model developed in this work provides a more efficient alternative for quantifying NAPL saturations using single-well push-pull test results when non-equilibrium mass transfer is important. Given that non-equilibrium partitioning into the NAPL is analogous to non-equilibrium sorption, sorption parameters in equations (1) and (2) can be redefined in terms of NAPL partitioning. The aquifer porosity (θ) must now be divided into the volume fraction of voids containing the aqueous phase (θ_a) and the volume of voids containing NAPL (θ_n). These volume fractions relate to the aqueous saturation (S_a) or NAPL saturation (S_n) according to $\theta_a = \theta S_a$ and $\theta_n = \theta S_n$, respectively. Given that only a fraction of the void space is now available for aqueous phase flow, θ should be replaced with θ_a , and assuming partitioning between the aqueous phase and NAPL is analogous to sorption, ρ_b should be replaced with θ_n in equation (1). Rate-limited mass transfer between the aqueous and NAPL phases is governed by the rate-limited mass transfer coefficient (α_{NAPL}) and the capacity for partitioning tracer to accumulate in the NAPL, which is governed by the aqueous phase-NAPL equilibrium distribution coefficient (K). With these substitutions, and assuming tracer injection is over the entire screen length, equation (1) becomes

$$r \left(\theta S_a \frac{\partial C}{\partial t} + \theta S_n \frac{\partial S}{\partial t} \right) = a_L q \frac{\partial^2 C}{\partial r^2} + q \frac{\partial C}{\partial r} + a_T q \frac{\partial^2 C}{\partial z^2} - r \theta S_a \lambda C - r \theta S_n \lambda S \quad (31)$$

and with only slight modifications in parameter nomenclature, the sorption solution described previously can be used to quantify the NAPL saturation in a system that includes non-equilibrium partitioning. This solution again uses the initial and boundary conditions expressed in equations (3) and (4) and is solved according to equation (15).

[33] To quantify the NAPL saturation, a number of parameters must be determined, including dispersivities and partitioning parameters. Longitudinal and transverse dispersivities (a_L and a_T) may be determined from the interpretation of non-partitioning (conservative) tracer test results as described previously. As before, the Darcy velocity (q) is computed from the aquifer thickness (M) and the well flow rate (Q). Partitioning parameters, i.e., the rate-limited mass transfer coefficient (α_{NAPL}) and the equilibrium distribution coefficient (K), may be determined from batch and column studies conducted in the lab using a sample of the NAPL collected from the field and the proposed partitioning tracers or, as shown in the following example, K may be determined in the lab while α_{NAPL} is estimated from the partitioning tracer field results. Likewise, aquifer porosity may be determined using conventional methods or may be simultaneously estimated from the tracer results, leaving the interpretation of the partitioning tracer extraction signal to quantify the NAPL saturation (S_n). While a reactive partitioning tracer could be used ($\lambda > 0$), it is advisable to use a non-reactive partitioning tracer to simplify the interpretation and analysis. The following section provides an example demonstrating the use of the

Table 4. Parameter Estimates Using a GA on Synthetic Data

Parameter	Simulation 1		Simulation 2		Simulation 3		
	Real ^a	Estimated	Real ^a	Estimated	Real ^a	Estimated	
Dispersivities ^b	a_L (m)	2.0	3.02	2.0	2.00	10.0	9.99
	a_T (m)	0.02	0.024	2.0	1.86	1.0	1.00
Adsorption Parameters ^b	α (d ⁻¹)	0.02	0.026	0.06	0.061	0.1	0.096
	k_d (L/kg)	3.0	2.49	8.0	7.13	1.0	0.94
NAPL Distribution Parameters ^b	θ	0.5	0.52	0.2	0.21	0.3	0.30
	S_n	0.08	0.09	0.05	0.074	0.01	0.015
	α_{NAPL} (d ⁻¹)	0.04	0.032	0.03	0.018	0.03	0.02

^a“Real” parameter values were used in the forward simulations to generate the synthetic concentration data that were then inverted using the GA coupled to the analytical solution methodology described in the text.

^bDispersivities and NAPL distribution parameter estimates were obtained after the GA ran for 40 generations; sorption parameter estimates required 120 GA generations.

proposed methodology to quantify the interrogated-volume average NAPL saturation.

6. Example

[34] As an example of model application, synthetic data were generated using typical parameter values found in the literature. The model was applied in a forward fashion using equation (18) to generate extraction well observations as a function of time. The model was then applied to these data in an inverse mode to estimate the original parameters. The inverse modeling process used in these applications is characteristic of many optimization problems. Here, the genetic algorithm (GA) developed by Carroll [1996] was used. The objective function for this model is given as

$$F_{obj} = \left(1 + \left[\frac{1}{N} \sum_{i=1}^N (C_2^O(t_i) - C_2^C(t_i))^2 \right]^{1/2} \right)^{-1} \quad (32)$$

where, $C_2^O(t_i)$ and $C_2^C(t_i)$ are the observed and modeled concentrations at time t_i , respectively. The GA determines the values of the model parameters (e.g., a_L , a_T) which maximize the objective function.

[35] The above-described procedure was applied to estimate (1) longitudinal and transverse dispersivities (a_L , a_T), (2) sorption parameters (α , k_d), and (3) NAPL distribution parameters (θ , S_n , α_{NAPL}) for three alternative simulation scenarios with parameters as depicted in Table 4 (“real” column). Note the simulations for sorption and NAPL distribution parameters are mutually exclusive. That is, either rate-limited sorption to aquifer solids or rate-limited partitioning into NAPL is assumed. Both processes do not occur in parallel, as we implicitly assume that if NAPL is present, partitioning into the NAPL would overwhelm any sorption to aquifer solids that may be occurring. Estimation of sorption and partitioning parameters is assumed to employ a fully screened well, such that transport can be assumed one-dimensional. For each simulation ($n = 1, 2, \text{ or } 3$), the GA was used to estimate the parameter values. Results are shown in Table 4 and Figure 7. As can be seen from Table 4, the estimated parameter values are generally within 20% of the “real” parameter values that were used to generate the synthetic data. Figure 7a demonstrates the quality of fit when using conservative tracer signals to estimate dispersivity only. As can be seen from Table 4, the poorest estimate was for the transverse dispersivity in simulation 1, which was overestimated by 20%. Note from Table 2 that

transverse dispersivity has the lowest CSS, so the inaccuracy of the estimate is not unexpected. In Figure 7b, the model provides an excellent fit to the simulation signals for the quantification of sorption parameters (α , k_d). Dispersivities are assumed known from conservative tracer signal interrogation. Figure 7c compares the best fit realization from the GA to each simulation in a NAPL source zone assumed to have relatively low, uniform NAPL saturations (see Table 4). Dispersivities are again assumed known from conservative tracer signal interrogation. Clearly the model is capable of fitting the “real” signals for these scenarios. As stated previously, however, results depicted in Figure 7c are limited to a conceptual model that assumes the saturation is uniformly distributed and would be incapable of recognizing nonuniformities in NAPL saturation. However, it is well recognized that this is a limitation in site characterization that is common for several characterization techniques (e.g., PITTs).

[36] It must be noted that to apply an analytical solution in the above scenarios, a number of relatively severe simplifying assumptions needed to be made. For instance, the synthetic parameters used in the above example are assumed to be homogeneous throughout the system, regional groundwater flow is assumed negligible, and both flow and transport are assumed to be radially symmetric. Obviously, a real system will have physical, chemical, and biological parameters that will vary in space (and perhaps even time) and asymmetric flow due to regional gradients and local heterogeneities. Figure 4 provides an example of the magnitude of the impact of spatial heterogeneity of just one parameter, hydraulic conductivity, on results. The accuracy of the analytical models presented here, which assume homogeneity and symmetry, will be strongly affected by the heterogeneity of the actual system’s parameters and the relative magnitude of regional flow. As an aside, one way to assess the goodness of the assumption of negligible regional flow is to compare the regional flow length-scale $\left(\frac{q_{reg} t_1}{\theta} \right)$, where q_{reg} is the regional flow Darcy velocity, with the push-pull experiment length-scale $\left(\sqrt{\frac{Q t_1}{\theta \pi (z_t - z_b)}} \right)$. Although

the simplifying assumptions required by an analytical model are severe, the models have value in that they offer a computationally efficient means of obtaining results. These models are quite useful in providing users with an easy mode of gaining insight into the interplay of different processes, as well as a way of checking results from the more

complex numerical models that might have to be applied during remediation design.

7. Conclusion

[37] The model developed in this work provides an efficient tool for the interpretation of single-well push-pull tracer test results. Applications for the estimation of longitudinal and transverse dispersivity, sorption parameters, and NAPL saturation and partitioning parameters demonstrate the utility of the model. The novel application of the model to estimate rate-limited partitioning to immobile NAPL for the estimation of in situ NAPL saturation provides a particularly attractive tool for estimating average NAPL source zone saturations. The incorporation of rate-limitations facilitates the application of this technology across a broader array of contaminated sites and overcomes the limitations of previous tracer interpretation models. The example demonstrates the coupling of this model with an optimization algorithm (GA) for the simultaneous estimation of aquifer and NAPL parameters, saving time and resources. This model provides an exciting new tool for aquifer characterization and will be relevant for a variety of environmental applications.

Appendix A: Derivation of Analytical Solution

[38] Applying Laplace transforms with respect to t (\bar{C}) and Finite Fourier Cosine transforms with respect to z (\hat{C}), equations (1) and (2) may be rewritten

$$a_L \frac{d^2 \hat{C}}{dr^2} - \frac{d\hat{C}}{dr} - [rf(p) + N(n)]\hat{C} = 0 \tag{A1}$$

where

$$f(p) = \frac{1}{q} \left[\theta(p + \lambda) + \frac{\alpha k_d \rho_b (p + \lambda)}{p + \lambda + \alpha} \right] N(n) = a_T \frac{n^2 \pi^2}{M^2}$$

and p and n are the Laplace and Finite Fourier Cosine transform parameters, respectively.

Letting $\hat{C} = y(x)e^{\frac{r-x}{2a_L}}$ and $x = a_L^{-1/3} \left(\frac{1}{4a_L} + rf + N \right) f^{-2/3}$ equation (A1) takes the form of the well-known Airy equation:

$$\frac{d^2 y}{dx^2} - xy = 0 \tag{A2}$$

which has the general solution [Abramowitz and Stegun, 1970]

$$y = c_1 Ai(x) + c_2 Bi(x) \tag{A3}$$

or

$$\hat{C} = c_1 e^{\frac{r-x}{2a_L}} Ai(x) + c_2 e^{\frac{r-x}{2a_L}} Bi(x) \tag{A4}$$

where $Ai(\cdot)$ and $Bi(\cdot)$ are the Airy functions.

[39] During stage 1, the Finite Fourier Cosine transform of the outer boundary condition (3c) is straight-forward and the inner boundary condition (3b) is

$$-\sigma a_L \frac{\partial \hat{C}}{\partial r} + \hat{C} = \frac{C_0}{p} \Lambda(n), \quad r = r_w \tag{A5}$$

where

$$\Lambda(n) = \frac{M}{n\pi} \left[\sin\left(\frac{n\pi z_t}{M}\right) - \sin\left(\frac{n\pi z_b}{M}\right) \right]$$

[40] Applying transformed boundary conditions (3c) and (A5), the constants in (A4) may be evaluated, resulting in

$$\hat{C}_1(r, n, p) = \frac{C_0}{p} \Lambda(n) e^{\frac{r-r_w}{2a_L}} \frac{Ai(x)}{\gamma_1 Ai(x_w) - \gamma_2 Ai'(x_w)}$$

The transformed concentration in the solid phase may likewise be written

$$\hat{S}_1(r, n, p) = \frac{\alpha k_d}{p + \lambda + \alpha} \hat{C}_1(r, n, p)$$

where the subscript 1 signifies solutions for stage 1 of the single-well push-pull test, and $\gamma_1 = 1 - \sigma/2$, $\gamma_2 = \sigma a_L^{2/3} f^{1/3}$ and $x_w = a_L^{-1/3} \left(\frac{1}{4a_L} + r_w f + N \right) f^{-2/3}$.

[41] To obtain the solution for the aqueous concentration in real time, equation (5) can be inverted using Appendices B and C. Assuming a constant concentration boundary condition ($\sigma = 0$),

$$\hat{C}_1(r, n, t) = C_0 \Lambda(n) e^{\frac{r-r_w}{2a_L}} F_{CC}(r, n, t)$$

and assuming a constant flux boundary condition ($\sigma = 1$),

$$\hat{C}_1(r, n, t) = C_0 \Lambda(n) e^{\frac{r-r_w}{2a_L}} F_{CF}(r, n, t)$$

where $F_{CC}(r, n, t)$ and $F_{CF}(r, n, t)$ are defined in Appendix B and C. In the special case where a tracer is injected for a pulse length t_s less than t_1 , the length of water injection during stage 1, the boundary condition (3b) may be rewritten using the Heaviside step function ($H(\cdot)$):

$$-\sigma a_L \frac{\partial C}{\partial r} + C = \begin{cases} C_0 H(t_s - t), & r = r_w, z_b \leq z \leq z_t \\ 0, & r = r_w, 0 \leq z < z_b, z_t < z \leq M \end{cases}$$

Solutions for this slightly modified scenario are readily obtained using superposition:

$$\hat{C}_1(r, n, t) = C_0 \Lambda(n) e^{\frac{r-r_w}{2a_L}} (F_{CC}(r, n, t) - F_{CC}(r, n, t - t_s)) \tag{A6}$$

for the constant concentration boundary condition and

$$\hat{C}_1(r, n, t) = C_0 \Lambda(n) e^{\frac{r-r_w}{2a_L}} (F_{CF}(r, n, t) - F_{CF}(r, n, t - t_s)) \tag{A7}$$

for the constant flux boundary condition.

[42] The solid phase concentration in real time can be obtained by inverting equation (6):

$$\begin{aligned} \hat{S}_1(r, n, t) &= \alpha k_d \int_0^t e^{-(t-\tau)(\lambda+\alpha)} \hat{C}_1(r, n, \tau) d\tau \\ &= C_0 \alpha k_d \Lambda(n) e^{\frac{r-r_w}{2a_L}} F_{conv}(r, n, t) \end{aligned}$$

where

$$F_{conv}(r, n, t) = F_{CC0}(r)\phi(t) - \frac{2}{\pi} \left(\int_{\xi_1}^{\xi_2} \frac{w(\xi, t)}{\xi} \Psi(r, n, \xi) d\xi + \int_{\xi_3}^{\infty} \frac{w(\xi, t)}{\xi} \Psi(r, n, \xi) d\xi \right)$$

for a constant concentration boundary condition ($\sigma = 0$), and

$$F_{conv}(r, n, t) = F_{CF0}(r)\phi(t) - \frac{4}{\pi} \left(\int_{\xi_1}^{\xi_2} \frac{w(\xi, t)}{\xi} \Omega(r, n, \xi) d\xi + \int_{\xi_3}^{\infty} \frac{w(\xi, t)}{\xi} \Omega(r, n, \xi) d\xi \right)$$

for a constant flux boundary condition ($\sigma = 1$), and where $\phi(t) = \frac{1}{\lambda + \alpha} [1 - e^{-(\lambda + \alpha)t}]$, $w(\xi, t) = \frac{1}{\lambda + \alpha - \xi^2} [e^{-\xi^2 t} - e^{-(\lambda + \alpha)t}]$, and all other parameters are as defined in the appendices.

[43] Finally, using the inverse Finite Fourier Cosine transform, the analytical solutions for concentrations in the aqueous and solid phase during stage 1 of the single-well push-pull test are obtained:

$$C_1(r, z, t) = \frac{1}{M} \hat{C}_1(r, 0, t) + \frac{2}{M} \sum_{n=1}^{\infty} \hat{C}_1(r, n, t) \cos\left(\frac{n\pi z}{M}\right)$$

$$S_1(r, z, t) = \frac{1}{M} \hat{S}_1(r, 0, t) + \frac{2}{M} \sum_{n=1}^{\infty} \hat{S}_1(r, n, t) \cos\left(\frac{n\pi z}{M}\right)$$

where \hat{C}_1 and \hat{S}_1 are as given in equations (10), (11), and (12).

[44] Solving for the aqueous and solid phase concentrations during stage 2, equation (1) may be rewritten using Laplace and Finite Fourier Cosine transforms (noting that the advection term is now positive, indicating convergent flow):

$$a_L \frac{d^2 \hat{C}}{dr^2} + \frac{d\hat{C}}{dr} - [rf(p) + N(n)] \hat{C} = -g(r, n, p) \quad (A8)$$

where $g(r, n, p)$ accounts for the nonzero initial conditions resulting from the stage 1 tracer push:

$$g(r, n, p) = \frac{r}{q} \left[\theta \hat{C}_1(r, n, t_1) + \frac{\rho_b \alpha}{p + \lambda + \alpha} \hat{S}_1(r, n, t_1) \right]$$

The homogeneous form of equation (A8) has two linear, independent solutions:

$$e^{-\frac{r}{2a_L} Ai(x)} \text{ and } e^{-\frac{r}{2a_L} Bi(x)} \quad (A9)$$

Green's function may be used to obtain the general solution to the heterogeneous form of equation (A8):

$$\hat{C} = c_1 e^{-\frac{r}{2a_L} Ai(x)} + c_2 e^{-\frac{r}{2a_L} Bi(x)} + H(r, n, p)$$

where c_1 and c_2 are the integration constants and $H(r, n, p)$ is the specific solution of (A8). Applying the boundary conditions (4b) and (4c), the solution to equation (A8) written in the transformed domains is

$$\hat{C}_2(r, n, p) = c_1(n, p) e^{-\frac{r}{2a_L} Ai(x)} + H(r, n, p)$$

where

$$c_1 = -\frac{\pi}{\gamma} \frac{Bi(x_w) - 2\gamma Bi'(x_w)}{Ai(x_w) - 2\gamma Ai'(x_w)} \int_{r_w}^{\infty} e^{\frac{r}{2a_L} Ai(x)} g(r, n, p) dr$$

$$H = \frac{\pi}{\gamma} e^{-\frac{r}{2a_L}} \left[Ai(x) \int_{r_w}^r e^{\frac{r}{2a_L} Bi(x)} g(r, n, p) dr + Bi(x) \int_r^{\infty} e^{\frac{r}{2a_L} Ai(x)} g(r, n, p) dr \right]$$

and $\gamma = a_L^{2/3} f^{1/3}$.

[45] Given that single-well push-pull tests employ solute concentrations extracted during stage 2 of the test to obtain aquifer parameters, it is important to quantify the concentration at the extraction well ($r = r_w$). For this condition, equation (7) simplifies to

$$\hat{C}_2(r_w, n, p) = \frac{2e^{-\frac{r_w}{2a_L}}}{Ai(x_w) - 2\gamma Ai'(x_w)} \int_{r_w}^{\infty} e^{\frac{r}{2a_L} Ai(x)} g(r, n, p) dr$$

or

$$\hat{C}_2(r_w, n, p) = \frac{e^{-\frac{r_w}{2a_L}}}{q} \int_{r_w}^{\infty} e^{\frac{r}{2a_L} \bar{F}_2(r, n, p)} r \left[\theta \hat{C}_1(r, n, t_1) + \frac{\rho_b \alpha}{p + \lambda + \alpha} \hat{S}_1(r, n, t_1) \right] dr$$

with $\bar{F}_2(r, n, p) = \frac{2Ai(x)}{Ai(x_w) - 2\gamma Ai'(x_w)}$ or using (C2), $\bar{F}_2(r, n, p) = p\bar{F}_{CF}(r, n, p)$.

[46] However, employing the Laplace transform of the derivative:

$$L\{F'_{CF}(r, n, t)\} = p\bar{F}_{CF}(r, n, p) - F_{CF}(r, n, 0)$$

where, $L\{\cdot\}$ indicates the Laplace transform and recognizing that $F_{CF}(r, n, 0) = 0$, the inversion of $\bar{F}_2(r, n, p)$ is

$$F_2(r, n, t) = F'_{CF}(r, n, t) = \frac{4}{\pi} \left(\int_{\xi_1}^{\xi_2} \xi e^{-\xi^2 t} \Omega(r, n, \xi) d\xi + \int_{\xi_3}^{\infty} \xi e^{-\xi^2 t} \Omega(r, n, \xi) d\xi \right) \quad (A10)$$

Using the convolution principle,

$$\hat{C}_2(r_w, n, t) = \frac{e^{-\frac{r_w}{2a_L}}}{q} \int_{r_w}^{\infty} e^{\frac{r}{2a_L} r} \left[\theta F_2(r, n, t) \hat{C}_1(r, n, t_1) + \Phi(r, n, t) \hat{S}_1(r, n, t_1) \right] dr$$

where

$$\Phi(r, n, t) = \rho_b \alpha \int_0^t e^{-(t-\tau)(\lambda + \alpha)} F_2(r, n, \tau) d\tau \quad (A11)$$

or

$$\Phi(r, n, t) = \frac{4\rho_b \alpha}{\pi} \left(\int_{\xi_1}^{\xi_2} \xi w(\xi, t) \Omega(r, n, \xi) d\xi + \int_{\xi_3}^{\infty} \xi w(\xi, t) \Omega(r, n, \xi) d\xi \right) \quad (A12)$$

Finally, using the inverse Finite Fourier Cosine transform, the final analytical solution for the solute concentration at

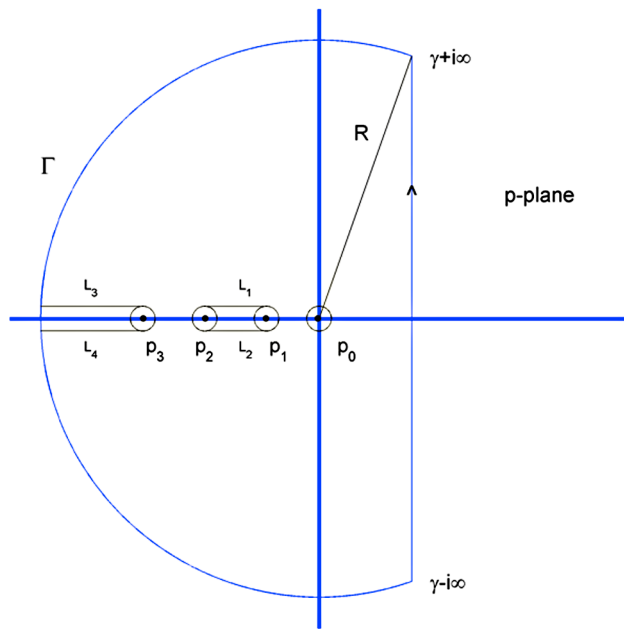


Figure B1. Modified Bromwich contour of integration for Laplace transform inversion.

the extraction well during stage 2 of the single-well push-pull test is

$$C_2(r_w, z, t) = \frac{1}{M} \hat{C}_2(r_w, 0, t) + \frac{2}{M} \sum_{n=1}^{\infty} \hat{C}_2(r_w, n, t) \cos\left(\frac{n\pi z}{M}\right)$$

where \hat{C}_2 is as given in equation (14).

Appendix B: Analytical Inversion of the Solution With Constant Concentration Boundary Conditions

[47] Setting $\sigma = 0$, equation (5) becomes

$$\hat{C}_1(r, n, p) = C_0 \Lambda(n) e^{\frac{r-r_w}{2aL} p} \bar{F}_{CC}(r, n, p) \tag{B1}$$

where

$$\bar{F}_{CC}(r, n, p) = \frac{1}{p} \frac{Ai(x)}{Ai(x_w)} \tag{B2}$$

Applying the complex inversion formula [Hildebrand, 1976], the inversion of (B2) to the real time domain may be written as

$$F_{CC}(r, n, t) = \frac{1}{2\pi i} \int_{\gamma-i\infty}^{\gamma+i\infty} \bar{F}_{CC}(r, n, p) e^{pt} dp \tag{B3}$$

[48] Following the inversion methodology employed by Chen [1985] with the intermediate variable $f(p)$ substituted for the Laplace parameter (p) in the expression for x_w , the Bromwich contour for the complex inversion may consider multiple branch points to account for the rate-limited adsorption process. Along the imaginary axis of the p plane, p has two segments, respectively on $[p_1, p_2]$ and $(-\infty, p_3]$, where, $p_1 = -\lambda$, $p_2 = -(\lambda + \alpha)$ and $p_3 = -(\lambda + \alpha) - \alpha k_d \rho_b / \theta$, that make $f(p)$ negatively valued, which are the cuts linking the branch points, p_1 , p_2 and p_3 . As indicated by

Abramowitz and Stegun [1970], the possible zeros of $Ai(x_w)$, which are the singular points of (B3), only distribute in the range $(-\infty < x_w < 0)$. The interesting interval are the cuts along $(p_2 < p < p_1)$ and $(-\infty < p < p_3)$. Based on this property, an improved Bromwich contour depicted in Figure B1 can be used to carry out the inversion. An equivalent integration path with $(\gamma - i\infty < p < \gamma + i\infty)$ is composed of $(\Gamma + L_1 + L_2 + L_3 + L_4)$. Thus, (B3) can be written

$$F_{CC}(r, n, t) = \sum_{i=0}^3 \text{Res}(p_i) + \frac{1}{2\pi i} \left(\int_{L_1+L_2+L_3+L_4+\Gamma} \right) \cdot F_{CC}(r, n, p) e^{pt} dp \tag{B4}$$

A unique nonzero residue is at $p_0 = 0$, which leads to

$$\sum_{i=0}^3 \text{Res}(p_i) = \frac{Ai(x_0)}{Ai(x_{w0})} \tag{B5}$$

where, x_0 and x_{w0} are the specific values of x and x_w , in which the intermediate variable $f(0) = \frac{1}{q} \left[\theta \lambda + \frac{\alpha k_d \rho_b \lambda}{\lambda + \alpha} \right]$. Since the integrand approaches zero when R , the radius of contour Γ , approaches infinity, there is no contribution along Γ . Along L_1 the integration is written as

$$\frac{1}{2\pi i} \int_{L_1} \bar{F}_{CC}(r, n, p) e^{pt} dp = -\frac{1}{\pi i} \int_{\xi_1}^{\xi_2} \frac{e^{-\xi^2 t}}{\xi} \frac{Ai(\eta e^{-2\pi i/3})}{Ai(\eta_w e^{-2\pi i/3})} d\xi \tag{B6}$$

where

$$\begin{aligned} \eta &= a_L^{-1/3} \left(\frac{1}{4aL} - rh + N \right) h^{-2/3} \\ \eta_w &= a_L^{-1/3} \left(\frac{1}{4aL} - r_w h + N \right) h^{-2/3} \\ h &= -\frac{1}{q} \left[\theta(\lambda - \xi^2) + \frac{\alpha k_d \rho_b (\lambda - \xi^2)}{\lambda + \alpha - \xi^2} \right] \\ \xi_1 &= \sqrt{\lambda} \\ \xi_2 &= \sqrt{\lambda + \alpha} \end{aligned}$$

Following Abramowitz and Stegun [1970],

$$Ai(\eta e^{-2\pi i/3}) = \frac{1}{2} e^{-\pi i/3} [Ai(\eta) + iBi(\eta)]$$

and the right hand side of (B6) takes the alternative form

$$\begin{aligned} &-\frac{1}{\pi i} \int_{\xi_1}^{\xi_2} \frac{e^{-\xi^2 t}}{\xi} \\ &\cdot \frac{Ai(\eta)Ai(\eta_w) + Bi(\eta)Bi(\eta_w) - i[Ai(\eta)Bi(\eta_w) - Bi(\eta)Ai(\eta_w)]}{Ai^2(\eta_w) + Bi^2(\eta_w)} d\xi \end{aligned} \tag{B7}$$

Along L_2 , the integration is of the negative conjugate of (B7). Combining L_1 and L_2 ,

$$\begin{aligned} &\frac{1}{2\pi i} \int_{L_1+L_2} \bar{F}_{CC}(r, n, p) e^{pt} dp \\ &= -\frac{2}{\pi} \int_{\xi_1}^{\xi_2} \frac{e^{-\xi^2 t}}{\xi} \frac{Ai(\eta)Bi(\eta_w) - Bi(\eta)Ai(\eta_w)}{Ai^2(\eta_w) + Bi^2(\eta_w)} d\xi \end{aligned} \tag{B8}$$

The contribution from L_3 and L_4 can be derived in the same way. Substituting these path integrations and residuals into (B4), the final inversion takes the form

$$F_{CC}(r, n, t) = F_{CC0}(r) - \frac{2}{\pi} \left(\int_{\xi_1}^{\xi_2} \frac{e^{-\xi^2 t}}{\xi} \Psi(r, n, \xi) d\xi + \int_{\xi_3}^{\infty} \frac{e^{-\xi^2 t}}{\xi} \Psi(r, n, \xi) d\xi \right) \quad (B9)$$

where

$$F_{CC0}(r) = \frac{Ai(x_0)}{Ai(x_{w0})}$$

$$\Psi(r, n, \xi) = \frac{Ai(\eta)Bi(\eta_w) - Bi(\eta)Ai(\eta_w)}{Ai^2(\eta_w) + Bi^2(\eta_w)}$$

$$\xi_3 = \sqrt{\lambda + \alpha(1 + k_d \rho_b / \theta)}$$

Substituting (B9) into (10), the solution in the real time domain is

$$\hat{C}_1(r, n, t) = C_0 \Lambda(n) e^{\frac{r-pw}{2aL}} F_{CC}(r, n, t)$$

Appendix C: Stage 2—Analytical Inversion of the Solution With Constant Flux Boundary Conditions

[49] Setting $\sigma = 1$, equation (5) becomes

$$\hat{C}_1(r, n, p) = C_0 \Lambda(n) e^{\frac{r-pw}{2aL}} \bar{F}_{CF}(r, n, p) \quad (C1)$$

where

$$\bar{F}_{CF}(r, n, p) = \frac{1}{p} \frac{2Ai(x)}{Ai(x_w) - 2a_L^{2/3} f^{1/3} Ai'(x_w)} \quad (C2)$$

Using complex inversion formula, the inversion of (C2) to the real time domain may be written

$$F_{CF}(r, n, t) = \sum_{i=0}^3 \text{Res}(p_i) + \frac{1}{2\pi i} \left(\int_{L_1+L_2+L_3+L_4+\Gamma} \right) \bar{F}_{CF}(r, n, p) e^{pt} dp$$

[50] In the same way as in Appendix B, the residuals are calculated according to

$$\sum_{i=0}^3 \text{Res}(p_i) = \frac{2Ai(x_0)}{Ai(x_{w0}) - 2a_L^{2/3} f_0^{1/3} Ai'(x_{w0})}$$

Chen [1987] demonstrated that the denominator of the second term on the right hand side of (C2) lacks a zero. Thus, the integration contour used in Appendix B may also be applied here. Along L_1 , if $p = \xi^2 e^{\pi i}$:

$$\frac{1}{2\pi i} \int_{L_1} \bar{F}_{CF}(r, n, p) e^{pt} dp = - \frac{2}{\pi i} \int_{\xi_1}^{\xi_2} \frac{e^{-\xi^2 t} Ai(\eta) e^{-2\pi i/3} / \xi}{Ai(\eta_w e^{-2\pi i/3}) - 2a_L^{2/3} h^{1/3} e^{\pi i/3} Ai'(\eta_w e^{-2\pi i/3})} d\xi \quad (C3)$$

where, following Abramowitz and Stegun [1970],

$$Ai(\eta e^{-2\pi i/3}) = \frac{1}{2} e^{-\pi i/3} [Ai(\eta) + iBi(\eta)] \quad (C4a)$$

$$Ai'(\eta e^{-2\pi i/3}) = \frac{1}{2} e^{\pi i/3} [Ai'(\eta) + iBi'(\eta)] \quad (C4b)$$

the right hand side of (C3) becomes

$$- \frac{2}{\pi i} \int_{\xi_1}^{\xi_2} \frac{e^{-\xi^2 t}}{\xi} \frac{Ai(\eta) + iBi(\eta)}{w_1 + iw_2} d\xi \quad (C5)$$

with

$$w_1 = Ai(\eta_w) + 2a_L^{2/3} h^{1/3} Ai'(\eta_w)$$

$$w_2 = Bi(\eta_w) + 2a_L^{2/3} h^{1/3} Bi'(\eta_w)$$

[51] Along L_2 , the integration is of the negative conjugate of (C5), which when combined with L_1 gives

$$\frac{1}{2\pi i} \int_{L_1+L_2} \bar{F}_{CF}(r, n, p) e^{pt} dp = - \frac{4}{\pi} \int_{\xi_1}^{\xi_2} \frac{e^{-\xi^2 t}}{\xi} \frac{Ai(\eta)w_2 - Bi(\eta)w_1}{w_1^2 + w_2^2} d\xi$$

Adding the contribution from L_3 and L_4 as well as the residual at $p_0 = 0$:

$$F_{CF}(r, n, t) = F_{CF0}(r, n) - \frac{4}{\pi} \left(\int_{\xi_1}^{\xi_2} \frac{e^{-\xi^2 t}}{\xi} \Omega(r, n, \xi) d\xi + \int_{\xi_3}^{\infty} \frac{e^{-\xi^2 t}}{\xi} \Omega(r, n, \xi) d\xi \right) \quad (C6)$$

where

$$F_{CF0}(r, n) = \frac{2Ai(x_0)}{Ai(x_{w0}) - 2a_L^{2/3} f_0^{1/3} Ai'(x_{w0})}$$

$$\Omega(r, n, \xi) = \frac{Ai(\eta)w_1 - Bi(\eta)w_2}{w_1^2 + w_2^2}$$

Substituting (C6) into (C1), the solution in the real time domain is obtained:

$$\hat{C}_1(r, n, t) = C_0 \Lambda(n) e^{\frac{r-pw}{2aL}} F_{CF}(r, n, t)$$

[52] **Acknowledgments.** Portions of this research were sponsored by the Strategic Environmental Research and Development Program, Project ER-1612 (contract W91HQ-08-C-0003). The content of this manuscript has not been subject to agency review and does not necessarily represent the view of the sponsoring agency. Additionally, the views expressed in this manuscript are those of the authors and do not reflect the official policy or position of the United States Air Force, Department of Defense, or the U.S. government.

References

Abramowitz, M., and I. A. Stegun (1970), *Handbook of Mathematical Functions*, Dover, New York.
 Anderman, E. R., M. C. Hill, and E. P. Poeter (1996), Two-dimensional advective transport in ground-water flow parameter estimation, *Ground Water*, 34(6), 1001-1009, doi:10.1111/j.1745-6584.1996.tb02165.x.
 Bear, J. (1979), *Hydraulics of Groundwater*, McGraw-Hill, New York.

- Brooks, M. C., M. D. Annable, P. S. C. Rao, K. Hatfield, J. W. Jawitz, W. R. Wise, A. L. Wood, and C. G. Enfield (2002), Controlled release, blind tests of DNAPL characterization using partitioning tracers, *J. Contam. Hydrol.*, *59*, 187–210, doi:10.1016/S0169-7722(02)00057-8.
- Carroll, D. L. (1996), Chemical laser modeling with genetic algorithms, *Am. Inst. Aeronaut. Astronaut. J.*, *34*(2), 338–346.
- Cassiani, G., L. F. Burbery, and M. Giustiniani (2005), A note on in situ estimates of sorption using push-pull tests, *Water Resour. Res.*, *41*, W03005, doi:10.1029/2004WR003382.
- Chen, C. S. (1985), Analytical solution and approximate solution to radial dispersion from an injection well to a geological unit with simultaneous diffusion into adjacent strata, *Water Resour. Res.*, *21*, 1069–1076, doi:10.1029/WR021i008p01069.
- Chen, C. S. (1987), Analytical solution for radial dispersion with Cauchy boundary at injection well, *Water Resour. Res.*, *23*(7), 1217–1224, doi:10.1029/WR023i007p01217.
- D'Agnes, F. A., C. C. Faunt, M. C. Hill, and K. Turner (1996), Death Valley regional groundwater flow model calibration using optimal parameter estimation methods and geoscientific information systems, in *Proceedings of the ModelCARE 96 Conference, Golden CO, September 1996, IAHS Publ.*, *237*, 41–52.
- Davis, B. M., J. D. Istok, and L. Semprini (2002), Push-pull partitioning tracer tests using radon-222 to quantify non-aqueous phase liquid contamination, *J. Contam. Hydrol.*, *58*, 129–146, doi:10.1016/S0169-7722(02)00010-4.
- Davis, B. M., J. D. Istok, and L. Semprini (2003), Static and push-pull methods using radon-222 to characterize dense non-aqueous phase liquid saturations, *Ground Water*, *41*(4), 470–481, doi:10.1111/j.1745-6584.2003.tb02381.x.
- Davis, B. M., J. D. Istok, and L. Semprini (2005), Numerical simulations of radon as an in situ partitioning tracers for quantifying NAPL contamination using push-pull tests, *J. Contam. Hydrol.*, *78*, 87–103, doi:10.1016/j.jconhyd.2005.03.003.
- Gelhar, L. W., and M. A. Collins (1971), General analysis of longitudinal dispersion in nonuniform flow, *Water Resour. Res.*, *7*(6), 1511–1521, doi:10.1029/WR007i006p01511.
- Goltz, M. N., and M. E. Oxley (1991), Analytical modeling of aquifer decontamination by pumping when transport is affected by rate-limited sorption, *Water Resour. Res.*, *27*(4), 547–556, doi:10.1029/90WR02760.
- Haggerty, R., M. H. Schroth, and J. D. Istok (1998), Simplified method of “push-pull” test data analysis for determining in situ reaction rate coefficients, *Ground Water*, *36*(2), 314–324, doi:10.1111/j.1745-6584.1998.tb01097.x.
- Haggerty, R., S. W. Fleming, L. C. Meigs, and S. A. McKenna (2001), Tracer tests in a fractured dolomite: 2. Analysis of mass transfer in single-well injection-withdrawal tests, *Water Resour. Res.*, *37*(5), 1129–1142, doi:10.1029/2000WR900334.
- Hall, S. H., S. P. Luttrell, and W. E. Cronin (1991), A method for estimating effective porosity and ground-water velocity, *Ground Water*, *29*(2), 171–174, doi:10.1111/j.1745-6584.1991.tb00506.x.
- Hellerich, L. A., P. M. Oates, C. R. Johnson, N. P. Nikolaidis, C. F. Harvey, and P. M. Gschwend (2003), Bromide transport before, during, and after colloid mobilization in push-pull tests and the implications for changes in aquifer properties, *Water Resour. Res.*, *39*(10), 1301, doi:10.1029/2003WR002112.
- Hildebrand, F. B. (1976), *Advanced Calculus for Applications*, 2nd ed., Prentice Hall, Englewood Cliffs, N. J.
- Hill, M. C. (1992), A computer program (MODFLOWP) for estimating parameters of a transient, three-dimensional, ground-water flow model using nonlinear regression, *U.S. Geol. Surv. Open File Rep.*, *91-484*, 358 pp.
- Hill, M. C., R. L. Cooley, and D. W. Pollock (1998), A controlled experiment in ground-water flow model calibration using nonlinear regression, *Ground Water*, *36*, 520–535, doi:10.1111/j.1745-6584.1998.tb02824.x.
- Hoopes, J. A., and D. R. F. Harleman (1967), Dispersion in radial flow from a recharge well, *J. Geophys. Res.*, *72*(14), 3595–3607, doi:10.1029/JZ072i014p03595.
- Huang, J., and C. Liu (1986), Analytical solution of partial differential equations for radial transport of a solute in double porous media, *Appl. Math. Mech.*, *7*, 327–336, doi:10.1007/BF01898222.
- International Mathematical and Statistical Library (2006), *IMSL Fortran Numerical Library User's Guide: Math/Library*, version 6.0, pp. 865–875 Houston, Tex.
- Istok, J. D., M. D. Humphrey, M. H. Schroth, M. R. Hyman, and K. T. O'Reilly (1997), Single-well, “push-pull” test for in situ determination of microbial activities, *Ground Water*, *35*(4), 619–631, doi:10.1111/j.1745-6584.1997.tb00127.x.
- Istok, J. D., J. A. Field, M. H. Schroth, T. E. Sawyer, and M. D. Humphrey (1999), Laboratory and field investigation of surfactant sorption using single-well, “push-pull” tests, *Ground Water*, *37*(4), 589–598, doi:10.1111/j.1745-6584.1999.tb01146.x.
- Istok, J. D., J. A. Field, and M. H. Schroth (2001), In situ determination of subsurface microbial enzyme kinetics, *Ground Water*, *39*(3), 348–355, doi:10.1111/j.1745-6584.2001.tb02317.x.
- Istok, J. D., J. A. Field, M. H. Schroth, B. M. Davis, and V. Dwarakanath (2002), Single-well “push-pull” partitioning tracer test for NAPL detection in the subsurface, *Environ. Sci. Technol.*, *36*, 2708–2716, doi:10.1021/es015624z.
- Jin, M. Q., M. Delshad, V. Dwarakanath, D. C. McKinnery, G. A. Pope, K. Sepehrnoori, C. E. Tilburg, and R. E. Jackson (1995), Partitioning tracer test for detection, estimation, and remediation performance assessment of subsurface nonaqueous phase liquids, *Water Resour. Res.*, *31*(5), 1201–1211, doi:10.1029/95WR00174.
- McDonald, M. G., and A. W. Harbaugh (1988), A modular three-dimensional finite difference groundwater flow model, in *Modeling Techniques, U.S. Geol. Surv. Water Resour. Invest., Book 6, Chap. A1*, 588 pp.
- Moench, A. F. (1989), Convergent radial dispersion: A Laplace transform solution for aquifer tracer testing, *Water Resour. Res.*, *25*(3), 439–447, doi:10.1029/WR025i003p00439.
- Pickens, J. F., and G. E. Grisak (1981), Scale-dependent dispersion in a stratified granular aquifer, *Water Resour. Res.*, *17*(4), 1191–1211, doi:10.1029/WR017i004p01191.
- Piessens, R., E. de Doncker-Kapenga, C. W. Uberhuber, and D. K. Kahaner (1983), *QUADPACK*, Springer, New York.
- Rodgers, J. L., and W. A. Nicewander (1988), Thirteen ways to look at the correlation coefficient, *Am. Stat.*, *42*, 59–66, doi:10.2307/2685263.
- Schroth, M. H., and J. D. Istok (2006), Models to determine first-order rate coefficients from single-well push-pull tests, *Ground Water*, *44*(2), 275–283, doi:10.1111/j.1745-6584.2005.00107.x.
- Schroth, M. H., J. D. Istok, and R. Haggerty (2000), In situ evaluation of solute retardation using single-well push-pull tests, *Adv. Water Resour.*, *24*, 105–117, doi:10.1016/S0309-1708(00)00023-3.
- Snodgrass, M. F., and P. K. Kitanidis (1998), A method to infer in situ reaction rates from push-pull experiments, *Ground Water*, *36*(4), 645–650, doi:10.1111/j.1745-6584.1998.tb02839.x.
- Tang, D. H., and D. K. Babu (1979), Analytical solution of a velocity dependent dispersion problem, *Water Resour. Res.*, *15*(6), 1471–1478, doi:10.1029/WR015i006p01471.
- Tang, D. H., and D. W. Peaceman (1987), New analytical and numerical solutions for the radial convection-dispersion problem, *Rep. 16001*, Soc. Pet. Eng., Richardson, Tex.
- Taskinen, A., H. Sirvio, and M. Bruen (2008), Generation of two-dimensionally variable saturated hydraulic conductivity fields: Model theory, verification and computer program, *Comput. Geosci.*, *34*, 876–890, doi:10.1016/j.cageo.2007.04.010.
- Tomich, J. F., R. L. Dalton Jr., H. A. Deans, and L. K. Shallenberger (1973), Single-well tracer method to measure residual oil saturation, *J. Pet. Technol.*, *25*, 211–218.
- Zheng, C., and P. Wang (1999), MT3DMS: A modular three-dimensional multispecies transport model for simulation of advection, dispersion, and chemical reactions of contaminants in groundwater systems, technical report, Waterways Exp. Stn., U.S. Army Corps of Eng., Vicksburg, Miss.
- Zlotnik, V. A., and J. D. Logan (1996), Boundary conditions for convergent radial tracer tests and the effect of well bore mixing volume, *Water Resour. Res.*, *32*(7), 2323–2328, doi:10.1029/96WR01103.

J. A. Christ, Department of Civil and Environmental Engineering, U.S. Air Force Academy, 2354 Fairchild Dr., Ste. 6J-159, USAF Academy, CO 80840, USA. (john.christ@usafa.edu)

M. N. Goltz, Department of Systems and Engineering Management, Air Force Institute of Technology, 2950 Hobson Way, Bldg. 640, Wright-Patterson Air Force Base, OH 45433-7765, USA. (mark.goltz@afit.edu)

J. Huang, Ground Water and Ecosystems Restoration Division, National Risk Management Research Laboratory, U.S. Environmental Protection Agency, Ada, OK 74820, USA. (huang.junqi@epa.gov)